Construction and Building Materials 407 (2023) 133565

Contents lists available at ScienceDirect

Construction and Building Materials

journal homepage: www.elsevier.com/locate/conbuildmat

A new method of seismic strengthening stone masonry with CRM coatings on one side

Natalino Gattesco [a], Emanuele Rizzi [a], Ingrid Boem [a], Allen Dudine [b], Matija Gams [c,*]

[a] University of Trieste, Department of Engineering and Architecture, Via Alfonso Valerio 6/1, Trieste 34127, Italy
[b] Fibre Net S.p.A., Via Jacopo Stellini, 3 – Z.I.U., Pavia di Udine (UD) 33050, Italy
[c] University of Ljubljana, Faculty of Civil and Geodetic Engineering, Jamova 2, Ljubljana 1000, Slovenija

ARTICLE INFO

Keywords:
Stone masonry
CRM reinforcement
Shear compression tests
Out-of-plane tests
Earthquake engineering

ABSTRACT

The paper presents the results of a research study aimed at assessing the effectiveness of composite-reinforced mortar (CRM) for the seismic strengthening of existing stone masonry walls. The experimental research focused on the strengthening performance of a coating applied only on one side of the masonry wall. Such an application is interesting because it does not require the temporary relocation of residents. The historic two-wythe stone masonry used in the research represents Adriatic's coastal and surrounding regions. The coating was made of hydraulic lime mortar reinforced with a glass fibre–reinforced polymer mesh attached to the wall using two types of anchors. In-plane cyclic shear compression tests and cyclic out-of-plane tests were conducted, and the performances of the coating on one and both sides were compared. The results showed that the coating on one side was effective, improving all aspects of the seismic response, which was successfully simulated using existing design models.

1. Introduction

The seismic resistance of existing masonry structures is relatively low because they were built before earthquake effects on structures were scientifically understood. Additionally, masonry has negligible tensile strength and low shear strength. The housing stock of such buildings is so large that it cannot be easily replaced, presenting a pressing need for effective and convenient methods of strengthening [1].

In Europe, the 1963 Skopje, present-day North Macedonia [2], and the 1976 Friuli, Italy, [3] earthquakes triggered much research on strengthening masonry structures. The key concept of strengthening by systematic structure tying using steel ties at the floor levels was scientifically developed and tested in that period. The ties connect walls and floors, redistributing seismic loads among elements of the entire structure and preventing its disintegration. It is also crucial for achieving 'box-like' behaviour [4]. The effectiveness of tying was confirmed by post-earthquake observations [5] and shaking table tests [6]. Tying using steel ties or other means is still the foundation of any seismic strengthening of masonry structures [7].

Even a proper box-like response of a masonry structure may be insufficient in the case of a strong earthquake because the existing masonry is inherently weak. The weakness results from the material's inability to resist tension, which usually occurs as a consequence of shear or even directly. Therefore, the masonry's strength in tension needs to be increased, typically achieved by adding materials with good tensile properties at locations where tension is expected. Steel was used for this purpose because it was the most cost-effective and readily available material.

In addition, coating masonry with steel-reinforced concrete or mortar is a traditional approach to strengthening masonry [5]. Despite desirable mechanical properties, several disadvantages of such strengthening exist. For instance, corrosion typically occurs fairly early because of the thin cover. The coating is usually thick (up to 6–8 cm), which reduces usable space on the inside, and prevents the preservation of important artistic façades on the outside. Furthermore, the application is invasive and dirty. When fibre-reinforced polymer (FRP) materials were introduced in construction, their potential for strengthening masonry was quickly recognised because of their excellent tensile properties, low weight, and ease of application.

Early attempts at using FRPs for seismic strengthening were made by Croci et al. [8] and Triantafillou [9]. Since then, significant research on this topic has been conducted. The first studies usually relied on using epoxy resin or, more generally, an organic matrix to provide the bond to the masonry. However, researchers later concluded that an organic

* Corresponding author.
E-mail address: mgams@fgg.uni-lj.si (M. Gams).

https://doi.org/10.1016/j.conbuildmat.2023.133565
Received 1 August 2023; Received in revised form 25 September 2023; Accepted 26 September 2023
Available online 2 October 2023

matrix was not the most suitable material for this task as it behaves poorly above the glass transition temperature and resists application on wet or cold surfaces. In addition, the material is not permeable [10] but significantly stronger than masonry, so the bond is the first to fail. The failure usually occurs in the substrate (masonry) in a 'peeling-off' type of failure [11]. Such failures have been repeatedly observed under simulated seismic loads in shear compression tests, as shown by Gams et al. [12] and many others for coating on one or both sides.

Therefore, the research community and practitioners have sought a more compatible material. Currently, studies focus more on the various combinations of advanced fibres in the form of textiles (with open-mesh configuration) with inorganic matrices, such as mortar coatings. Such systems are generally collected under the acronym TRM (textile-reinforced mortar). Different combinations of matrix and reinforcement result in different TRM composites, e.g. FRCM (fibre-reinforced cementitious matrix) and CRM (composite-reinforced mortar). These two macro-categories differ in their combined materials: FRCM uses thin, high-performance cement-based plaster (<15 mm) and fibre meshes of reduced size (<30 mm), usually made of dry fibres; CRM is the application of a thicker coating of medium–low–performance mortar and larger fibre meshes, usually resin-impregnated.

Papanicolaou et al. performed a large-scale test campaign on TRM [13,14], focusing on hollow clay masonry. Research into TRM has accelerated since, as summarised in recent papers by De Santis et al. [15] and Kouris and Triantafillou [16]. Additionally, TRM research examined different scale levels, ranging from single material components [17] to masonry walls and structures [18]. The tests on full-scale TRM-strengthened masonry elements are particularly significant, as they explain the resisting mechanisms in structures under realistic boundary and loading conditions and the actual interaction among layers. For example, cyclic in-plane shear-compression tests [19,20] and out-of-plane (OOP) bending tests [21,22].

Despite using mortar with a reduced elastic modulus designed specifically for strengthening applications, a CRM-strengthened wall consists of two substantially different materials. The coating is homogeneous and strong in tension, exhibiting a large displacement and inelastic deformation capacity and high stiffness at the material level. The masonry, on the other hand, lacks or has the opposite of these properties. In strengthening, we merge these two materials and expect them to cooperate and respond as a perfect composite member until near collapse. The difficulty lies, therefore, in achieving proper interaction, avoiding undesired collapse mechanisms and exploiting both materials as much as possible.

The differences between the materials produce an exceptionally high demand on the coating-to-masonry bond. The stress is increased further by lateral load reversals that occur during earthquakes in addition to the compressive load. These two effects usually cause the wall to shrink slightly during an earthquake, a deformation that the coating cannot easily follow [12], potentially causing catastrophic failure. The significant demands on the bond require mechanical anchors to improve the connection, especially after the original bond is lost. The requirement of anchors is typically observed in research based on cyclic shear compression tests [23,24]. Furthermore, these challenges require validation of a strengthening system that can only be accomplished through experimental testing under simulated shear compression loads.

Normally, the CRM coating is applied on both sides of the wall and anchored with connectors running through the entire wall thickness. Such a 'sandwich' application displays obvious mechanical benefits and reduces the demand on the bond. However, it requires full access to the wall on both sides, which is very inconvenient for residents, who are usually required to move out for the duration of the construction works. Therefore, the structure owners are quite reluctant about such interventions and may postpone them or consider other solutions, such as demolition and replacement construction. In the former case, the situation presents a clear risk to the residents and their economic well-being because they live in seismically vulnerable structures. In the latter case, the cost of replacing the building is considerable in terms of money, resource use, and, by extension, emissions.

The present research aims to develop and test a strengthening intervention that does not require the temporary removal of residents, making the decision for seismic strengthening more appealing. A CRM type of strengthening for stone masonry that is applied only on one side is proposed with special anchoring to avoid the aforementioned bond problems and prevent the separation of the masonry leaves. The strengthening system is tested by full-scale tests under in-plane cyclic shear compression and OOP bending tests. The performance of the developed strengthening system is also estimated with design models, further validating its efficiency.

2. Experimental programme

2.1. Scope and methods

As indicated in the introduction, strengthening walls by applying the reinforced coating on only one side of the wall is much more appealing than that on both sides simply because it does not require residents to move out for the duration of the construction works. However, we do not know if coating and historic stone masonry walls can work together as a composite element under such intense load conditions as seismic loads. Therefore, the main objective of the experimental programme is to analyse whether the strengthening solution with anchored CRM coating on one side of the wall increases the seismic response and to quantify the effect. The effect of strengthening is assessed by comparing unstrengthened walls with walls strengthened on one and two sides. Three in-plane tests and one OOP test were performed on full-scale samples to study the strengthening effect comprehensively. The experimental tests presented in Table 1 were carried out at the University of Trieste (Italy).

The tests on the masonry piers were part of a more extensive test campaign within the Interreg CONSTRAIN Project, which included various tests on materials, shear-bending tests on spandrels, tests on the performance of ties, OOP tests of top bond beams and full-scale cyclic tests on a two-storey rubblestone masonry building.

2.2. Materials and construction

The stone masonry piers were constructed to replicate typical historic masonry with weak lime mortar. A specially designed mixture of natural hydraulic lime (NHL) and sand was used for construction, with a granulometric distribution similar to that found in existing masonry buildings [25]. The mass ratio of lime to sand was 1:7 (200 kg hydraulic lime and 1400 kg of sand per m^3 of mortar). The grain size distribution of the aggregate ranged between 0.05 and 3 mm, and about 45 % of the sand was smaller than 0.5 mm. The bending and compressive strengths were determined on twelve standard 160×40×40 mm prisms sampled at regular intervals during construction. The tests were performed according to EN 1015–11 [26]. The main results are summarised in

Table 1
Experimental programme.

Type of test	Masonry type	Label*	Strengthening
Shear compression tests on masonry piers	Stone	P-R2U	None
	Stone	P-R2R-1	CRM on one side
	Stone	P-R2R-2	CRM on two sides
OOP bending tests on piers	Stone	B-R2	CRM on one side

* P/B – shear compression/bending, R2 – two-wythe rubble stone masonry, U/R1/R2 – unreinforced/strengthened on one side/strengthened on both sides.

Table 2
Mechanical properties of the mortars (*CoV* – coefficient of variation).

Property of mortar	Mean [MPa]	*CoV* [%]
Masonry mortar		
Flexural tensile strength	0.17	14.9
Compressive strength	0.93	4.4
Coating mortar		
Flexural tensile strength	3.44	4.2
Compressive strength	15.27	10.9
Elastic modulus	10 091	2.66

Table 2.

The stone masonry was built with a mix of Berrettino and Medolo Credaro stones, with approximate compressive strengths of 170 and 150 MPa, respectively. These stones are sandstone type with a calcareous composition. Berrettino is a mainly carbonate (calcarenite) rock made of minute detrital grains with evident stratification and a yellow-brown or pink colour. In contrast, Medolo comprises almost entirely microcrystalline calcium carbonate (crystalline limestone) with a very fine grain size and a hazelnut-grey colour. The rocks were hewn to blocks with average dimensions (depth × height × length) of 150×90×230 mm, with substantial variability.

All samples were constructed using the same technique with extra effort to simulate the mechanical response of historic masonry. The walls were built as 350 mm–thick two-leaf walls without any connector stones, and the space between the leaves was loosely filled with mortar and smaller rocks. The compressive strength and elastic modulus were measured on masonry prisms with dimensions of 0.50×0.35×1 m according to EN 1052–1 [27]. The compressive strength f_c and elastic modulus (at one-third of the maximum force) E of the masonry were 2.48 and 1074 MPa, respectively. Compressive failure was achieved at 1.2 % axial strain.

The piers were strengthened using a CRM coating, which was applied to the surface manually. The mortar was a commercial product specifically designed for strengthening masonry. The natural hydraulic lime mortar coating was about 30 mm thick. Samples for testing were taken regularly during construction, and compressive and flexural strengths were measured on six 160×40×40 mm prisms according to EN 1015–11 [26]. Four cylindrical samples, with dimensions diameter/length = 100/200 mm were tested in accordance with EN 12390–13 [28] to determine the elastic modulus of the coating mortar at one-third of the rupture load. The main mechanical characteristics are summarised in Table 2.

The mortar coating was reinforced with a glass fibre-reinforced polymer (GFRP) mesh, composed of twisted fibre wires in the warp direction weaved on parallel fibre wires in the weft direction. The mesh was placed on the wall, and spacers were provided between the wall and the mesh so that the mesh was positioned approximately at the middle of the coating. Tensile tests were carried out on the GFRP wires to determine the tensile strength and axial stiffness, according to ISO 10406 [29], as summarised in Table 3. The mesh spacing was 66×66 mm, and the specific density was 420 g/m^2. The modulus of elasticity, according to the producer, was 25 GPa.

The coating was fastened to the wall with connectors. For the coating applied on both sides, only L-shaped solid GFRP connectors were used (Fig. 1a, Fig. 2a). For the coating on only one side, injected steel connectors were used in addition to the GFRP anchors (Fig. 1b, Fig. 2b).

The L-shaped solid GFRP connectors were bars with a 10×7 mm cross-section and a nominal fibre cross-sectional area of 32.4 mm^2. The nominal characteristic tensile strength of connectors was 300 MPa, the elastic modulus was 21.4 GPa, and the ultimate strain was 1.9 %. The long side of the anchor, which was 300 mm long, was inserted into the wall using a two-component vinylester chemical anchor. For the coating on both sides of the wall, a 24 mm–diameter hole was bored through,

Table 3
Properties of the GFRP wires – nominal dry fibre cross-section A_{fib}, tensile resistance T_w, ultimate strain ε_u and axial stiffness k.

Property	Mean	*CoV* [%]
Twisted mesh wires – 66 × 66 mm mesh pitch		
A_{fib}	3.70 mm^2	–
T_w	5.11 kN	2.4
ε_u	1.85 %	1.9
k	3.95 kN/mm	2.62
Parallel mesh wires – 66 × 66 mm mesh pitch		
A_{fib}	3.70 mm^2	–
T_w	5.93 kN	3.9
ε_u	2.03 %	4.2
k	4.16 kN/mm	1.62

and the connectors were inserted from both sides. The connectors from both sides overlapped in the middle by at least 200 mm. In the case of the coating on one side, a 16 mm hole was bored, and the connectors were inserted to a depth of 300 mm. The short side of the connector, which was 100 mm long, held the mesh to the wall. In front of each connector, a GFRP mesh sheet (150×150 mm) with a 33×33 mm grid dimension was positioned to distribute stresses between the coating and the connector. Six connectors per m^2 were installed uniformly over the entire surface.

An injected steel connector was used for additional anchoring in walls with the coating only on one side. These were manufactured on-site by core-drilling a 50 mm–diameter hole into the wall, installing a threaded M16 steel bar and injecting the bar with high-strength thixotropic mortar. In addition to connecting both leaves of the wall, the injected steel connectors anchor the coating to the wall. The anchoring effect was achieved by installing a 150 mm–diameter circular steel plate (washer) on top of the injected steel connector (Fig. 1b, Fig. 2b). When both types of connectors were used, the anchor density was four L-shaped connectors per m^2 and two injected steel connectors per m^2. The total density of connectors remained at 6/m^2.

All the samples were constructed in the laboratory. First, the masonry was constructed and after curing for at least four weeks, the coating was applied. The coating was left to cure as well, and afterwards the samples were transported to the test apparatus. The walls were unloaded during application of the coating, as in e.g. Tomaževič et al. [30] among others.

2.3. Test setups, instrumentation and procedure

2.3.1. In-plane tests

The stone masonry piers were tested under conditions simulating earthquake loads. The walls were subjected to constant compression and cyclic in-plane lateral loads. The boundary conditions on the wall were fixed–fixed, preventing rotation at the top and bottom.

The two leaf stone piers were built without connector stones to simulate historical construction but with proper longitudinal overlapping of rocks between rows. The dimensions of the piers, shown in Fig. 3, were 1500×1960×350 mm (length × height × thickness). The unstrengthened sample pier is illustrated in Fig. 3a, and the sample strengthened on one side is shown in Fig. 3b. The test setup for the in-plane response of piers is illustrated in Fig. 4a. Each masonry specimen was built on a reinforced concrete (RC) element (1.50×0.35×0.30 m); the steel stirrups of the concrete element were welded to a holed, 20 mm–thick steel plate. The steel plate was connected to a welded steel profile, fixed to the laboratory's strong floor by two steel tie rods, 50 mm in diameter, 1000 mm apart, and each pretensioned to 140 kN. A second RC element with the same dimensions was placed on the top of the masonry specimens and connected to the stiff steel beam of the test setup. The top steel beam was used to apply both vertical and horizontal forces to the tested masonry walls. The loads on the beam were imposed

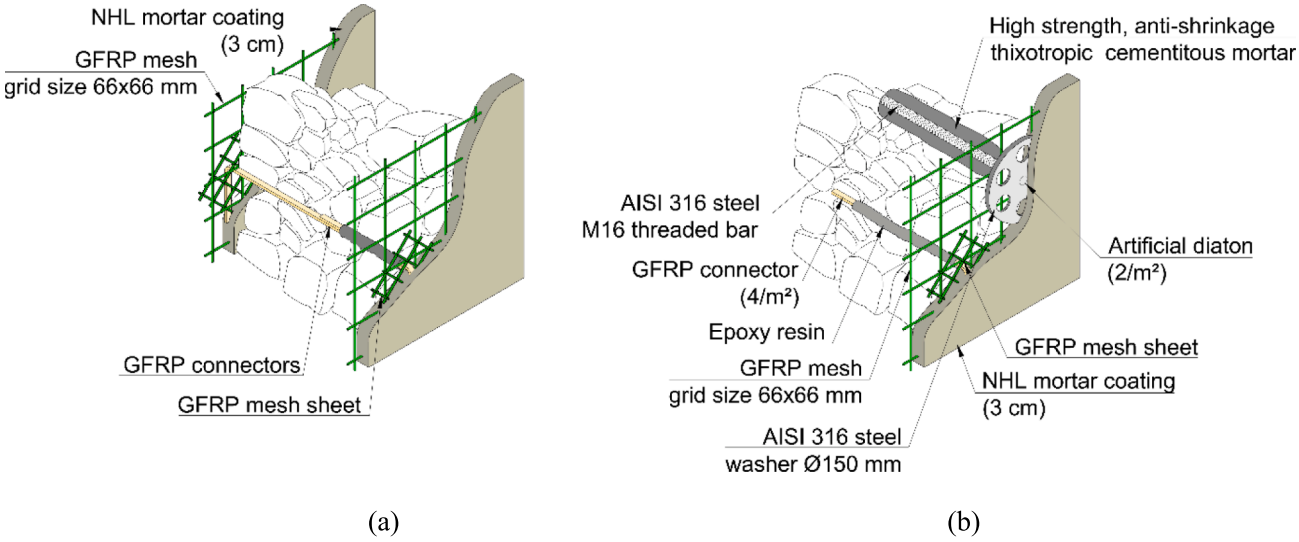

Fig. 1. CRM strengthening system – (a) two-sided and (b) one-sided strengthening.

Fig. 2. View of the connectors during construction: (a) L-shaped GFRP connectors before application of coating and (b) artificial diatone during application of coating.

using electro-mechanical jacks. One jack was used for horizontal (seismic) loads, and two jacks applied the vertical loads. During the tests, the two steel rods prevented OOP displacements at the upper RC element level. The rods were connected to an external fixed support.

Each specimen was equipped with 19 displacement transducers, as shown in Fig. 4b. The transducers measured lateral displacements, axial and shear deformations, uplift and slip relative to the foundation. In particular, transducers T0/T2 and T1/T3 measured the diagonal variation on both faces of the specimen. Transducers T4/T6 and T5/T7 surveyed the vertical deformation of the specimen at the left and right vertical edges, respectively. The vertical displacement between the specimen's first masonry row and the floor was measured using transducers T8 and T9, while the uplift of the stiff steel beam at the top of the specimen was monitored with transducers T10 and T11. In addition, transducers T12 and T13 monitored the distance between the top steel beam and the floor. Simultaneously, the masonry–concrete slip at the top and bottom edges of the specimen was surveyed via transducers T14 and T15. Transducer T16 was designated for measuring the slip of the bottom concrete element relative to the floor base steel beam. Transducers T17 and T18 measured the horizontal displacement at the top of the specimen. Finally, vertical and lateral forces were measured by three load cells.

A digital image correlation (DIC) system measured the displacement and strain fields on one wall surface. The side facing the cameras of the DIC system was painted with a contrasting random speckle pattern, and the other side was painted white to facilitate the visual examination of cracks.

First, the vertical load was applied by the two actuators at the sides of the wall. This load was gradually increased until the desired stress state of 0.5 MPa was attained, corresponding to about 20 % of the masonry compressive strength. Because the coating was applied before the specimens were loaded in compression, the application of vertical load induced stresses in the bond between the masonry and the coating that are not present in reality. These additional stresses in the tests have a negative impact on the performance of the coating, and the tests are thus considered conservative from this point of view.

Next, a lateral load was applied by imposing displacements at the top of the wall. The software controlled vertical jacks so that the total vertical load was constant and the vertical displacements on transducers T12 and T13 were the same throughout the test. The lateral load was cyclic, and each displacement amplitude was applied in the positive and negative directions. Because of the slow speed of the electro-mechanical actuators, each load amplitude was only repeated once (instead of the usual three times) before it was increased. The load protocol was based on procedures usually used to simulate seismic loads [31,5] and the authors' experience. The test was performed until we feared imminent

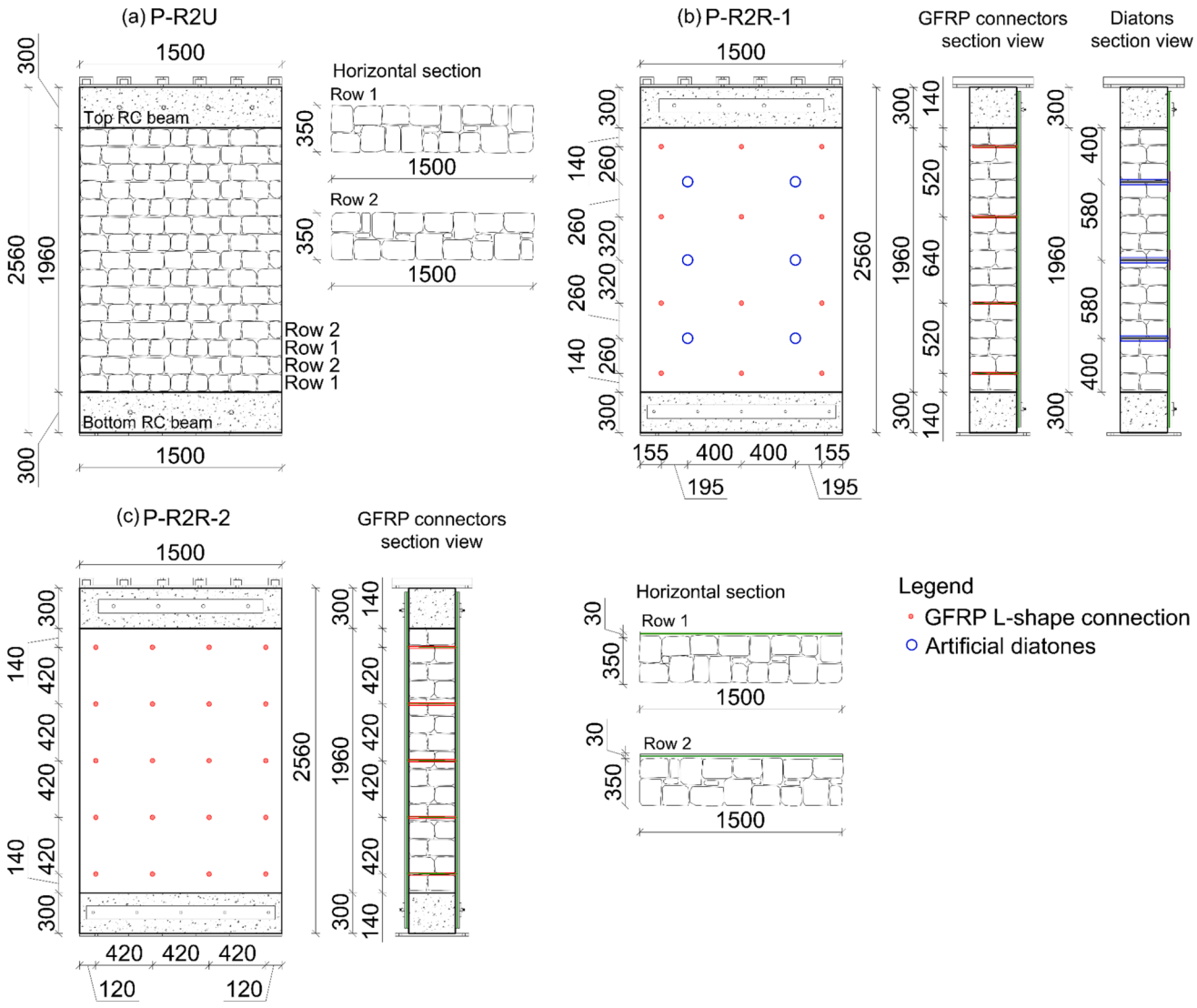

Fig. 3. Lateral and cross-sectional views of sample (a) P-R2U and (b) P-R2R-1 and (c) P-R2R-2 (dimensions in mm).

collapse, corresponding to the so-called near collapse limit state. The loading cycles are shown in Fig. 5.

2.3.2. *Out-of-plane tests*

The OOP test was performed to examine the effect of reinforced coating on the OOP response of the walls. The specimen was constructed in the same way as those for in-plane tests but with dimensions of 1030×2480×350 mm (length × height × thickness). The sketch of the wall and the coating is presented in Fig. 6.

The test setup for the OOP response of piers is illustrated in Fig. 7a. It consisted of a steel truss reaction wall, restraining bars for the wall specimen, a trolley for the load distribution beams and a hydraulic actuator. The test setup was a vertical three-point bending test with the samples free to rotate at the top and bottom.

As seen in Fig. 6 and Fig. 7, an RC block was at the top and bottom of the pier. A smooth horizontal Ø40 mm steel bar ran through each RC block, and the block was connected to the reaction wall by horizontal steel bars. At the bottom, the hinge joints rested on two steel profiles, which bore the entire weight of the specimen.

To transfer the load, two HEA 160 steel beams, connected at the ends, were placed horizontally at both faces of the specimen at half height. They were kept in place by a trolley on ball bearings. Between the HEA 160 beams and the specimens were loading plates, which were free to rotate.

Since no compression was acting in the walls and the friction between the RC blocks and the wall was relatively low, steel tubular tensioners were installed to increase the friction and prevent shear slip at the RC block–masonry interface. These devices, shown in Fig. 8, increased friction via compression between the blocks and the wall by manually tightening the nuts.

Each specimen was equipped with 13 displacement transducers, as shown in Fig. 7b, and a load cell to measure the force in the actuator. The DIC system measured the displacement and strain fields on one wall surface. The side facing the cameras with the optical system was painted with a contrasting random speckle pattern, and the other side was painted white to facilitate visual examination of cracks.

The load in the actuator was controlled by regulating the oil pressure with a manual pump and applied cyclically in positive and negative directions. The first cycles were performed by controlling the force. When the first crack appeared on the reinforced side, we switched to displacement control. Each displacement amplitude was applied once in the positive and negative directions before it was increased. After crack opened on the unstrengthened side and load stopped increasing with increasing displacement, the load was applied monotonically toward the reinforced side until failure. The loading cycles are reported in Fig. 9.

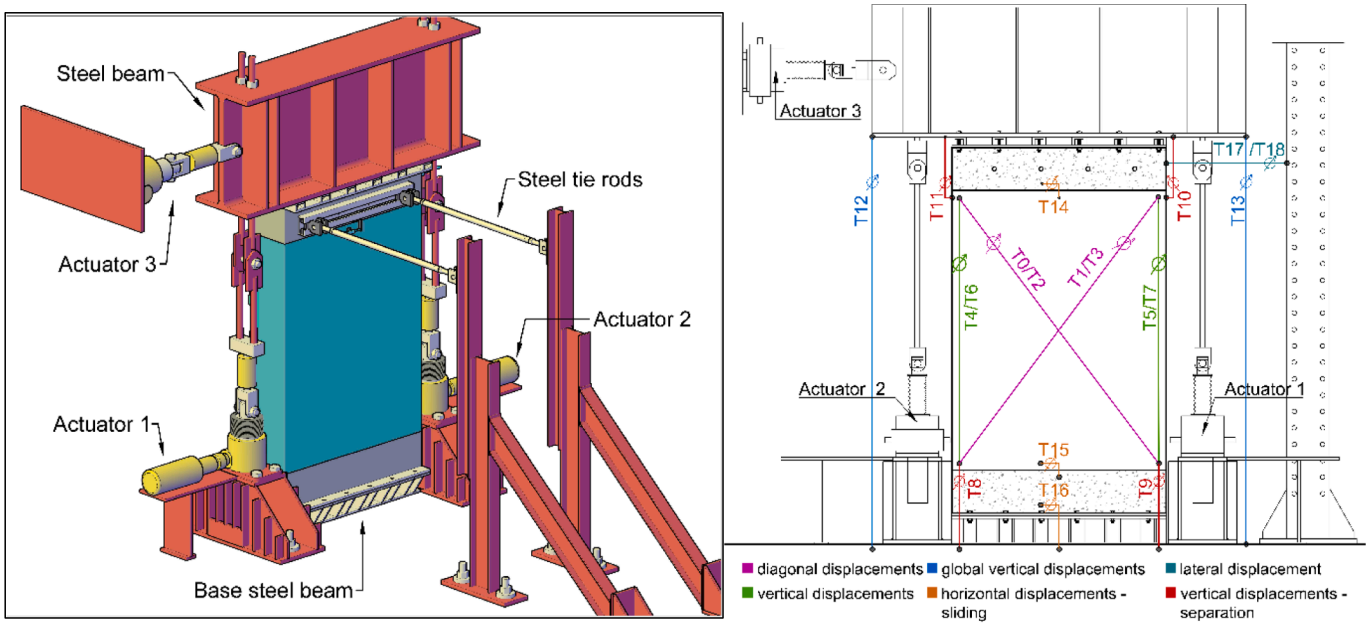

Fig. 4. Test setup and instrumentation for in-plane shear-compression tests – (a) front view and (b) instrumentation.

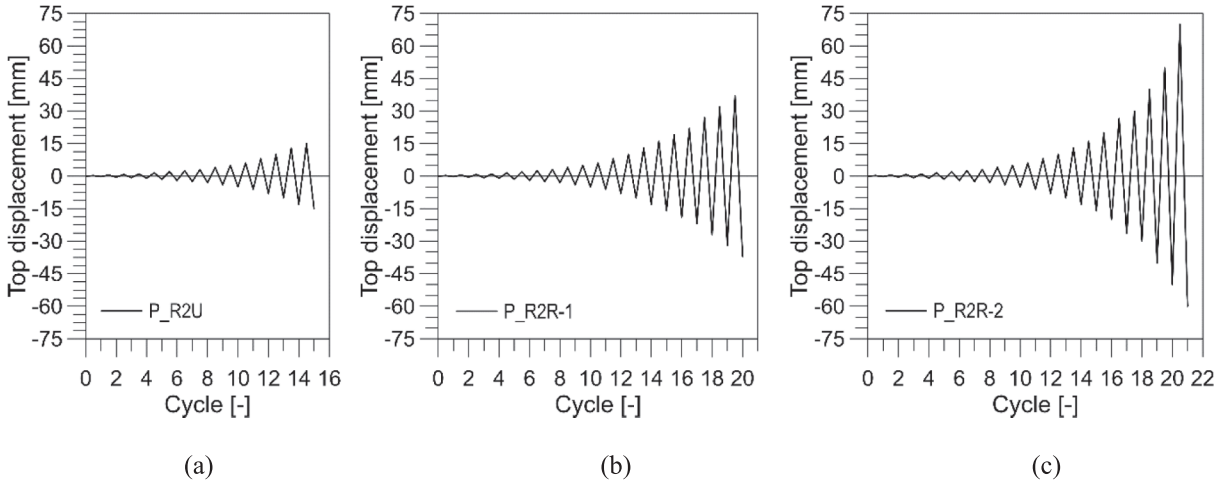

Fig. 5. Loading cycles for the piers (a) unreinforced, (b) reinforced on one side and (c) and two sides.

3. Results and discussion

3.1. In-plane tests

3.1.1. Seismic response, collapse mechanisms and limit states

The unreinforced stone masonry pier (P-R2U) responded in shear, characterised by diagonal cracks, which is a well-known mechanism [5]. The first damage in the wall was observed at a drift of 0.10 % and a lateral force of 81 kN. The first cracks were inclined, appearing in the middle of the wall. Maximum resistance was attained at 0.24 % drift and 108 kN, whereas the test was stopped at 0.75 % drift and 63 kN. The damage pattern at the end of the experiment is shown in Fig. 10a and d.

The wall strengthened on one side (P-R2R-1) had minor cracks in the first mortar bedding and at the base of the coating before the beginning of the test, causing a lower-than-expected initial stiffness, which was quite similar to that of the unstrengthened sample. During the test, damage developed differently on the strengthened and unstrengthened sides (Fig. 10b and e). The response and damage on the unstrengthened side were again in shear, which was clear from the diagonal cracks.

On the other hand, on the strengthened side, the cracks in the coating were almost vertical initially, only starting to incline after maximum resistance was reached. At that point, horizontal cracks in the coating appeared, indicating the starting of bending. Despite these horizontal cracks, the governing mechanism was shear. The cracking in the unstrengthened side was concentrated in one large crack, whereas the cracking in the coating was spread out in many parallel cracks. The high number of cracks in the coating is believed to be the reason for the increased energy dissipation capacity of the strengthened wall. Finally, at near collapse, the entire coating lost contact with the masonry, except where connectors were present. Ultimately, the coating near the injected steel connectors crumbled, and the GFRP mesh fractured. The first cracks appeared simultaneously on both sides at about 0.1 % drift and 83 kN lateral force. At a maximum resistance of 159 kN, the drift was 0.66 %, and at near collapse, the resistance and drift were 94 kN and 1.76 %,

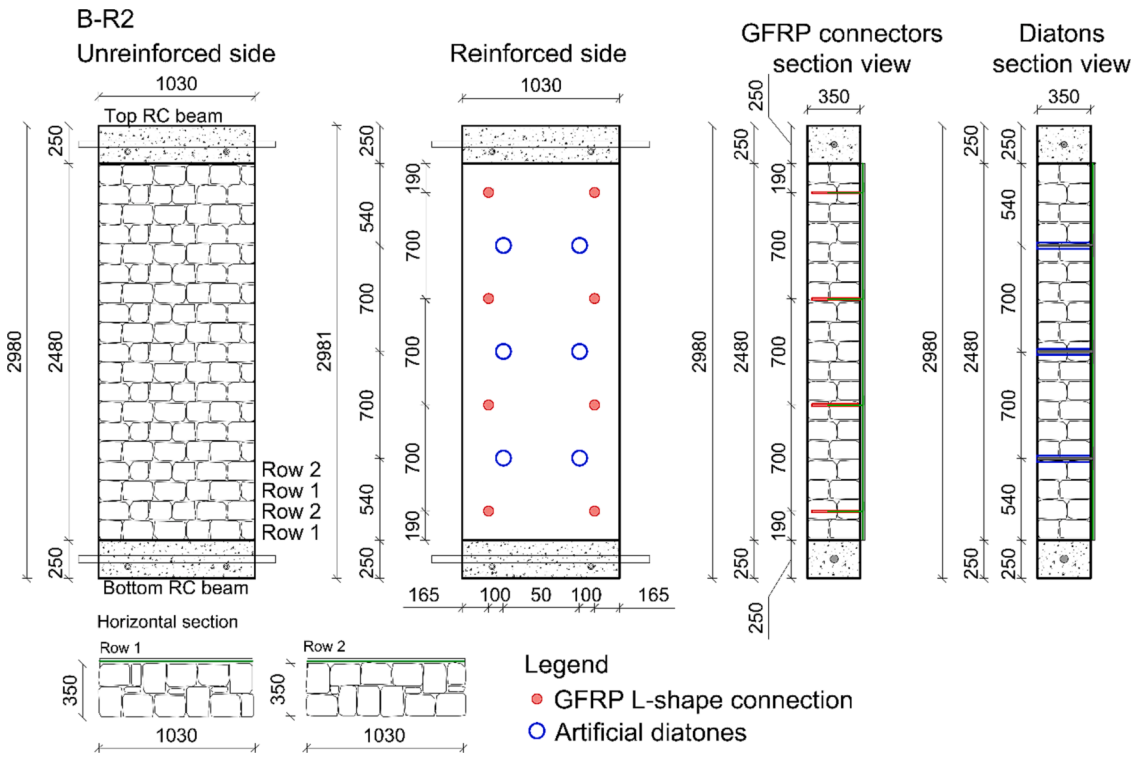

Fig. 6. Test specimen for OOP.

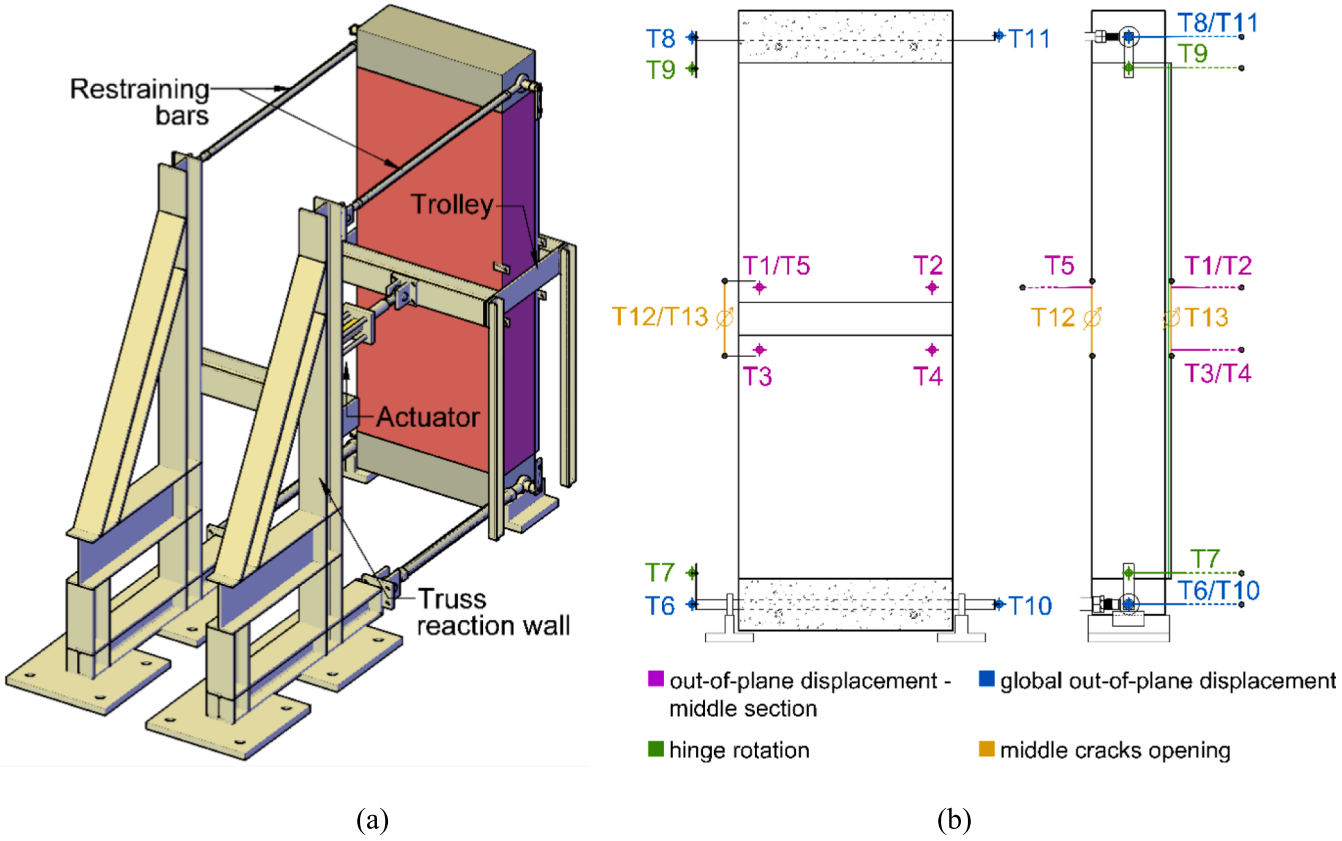

Fig. 7. Test setup for OOP tests – (a) rear view and (b) instrumentation.

Fig. 8. Steel tie rods at the top and bottom of the pier – (a) front view and (b) rear view.

respectively.

The first cracks (at 0.2 % drift and 160 kN) in the pier strengthened on both sides (P-R2R-2) were horizontal cracks at the bottom and top, indicating the start of bending damage (Fig. 10c and f). The bending response remained dominant throughout the test, including at peak resistance (at 1 % drift and 228 kN). Despite the apparent bending response, the coating had many inclined cracks. Horizontal and inclined cracks were spread over a large area, substantially increasing the energy dissipation capacity. Even at near collapse (3 % drift and 158 kN), when the coating lost all connection with masonry except by connectors, the damage was a combination of shear and bending. A vertical crack between the wythes developed at 1 % drift and gradually widened until the end of the test.

The limit states for all three walls are presented in Table 4, and the effect of strengthening relative to the unstrengthened state is shown in Table 5. As expected, the two-sided strengthening was substantially better than the single-sided, owing to the twice-as-thick, symmetric coating and double the GFRP mesh reinforcement. The single-sided coating still performed significantly better than the reference wall in all categories except the cracking limit state.

No appreciable OOP response was observed in any of the three cases, which was contrary to expectations, as the coating on one side created a considerable asymmetry with respect to the middle plane of the wall.

The hysteretic response of all three piers is compared in Fig. 11. The skeleton curves of each specimen are shown, allowing for a better comparison in terms of stiffness, resistance and maximum displacement capacity.

3.2. Stiffness degradation

To evaluate the stiffness (K) degradation, the slope of the peak-to-peak line within the first loop at each displacement level of the base shear–lateral displacement curves was calculated. Despite the system being designed to be rigid, appreciable displacements were observed by instruments T8/T9 and T10/T11 at the base and top of the wall, respectively. This resulted in the walls not behaving as fully fixed in all of the samples and a certain level of rotation of the bottom and top concrete beams. Thus, the real stiffness was derived by accounting for the displacements due to rotations.

A reference experimental initial stiffness of the unstrengthened wall (K_{ref} = 59.7 kN/mm) was evaluated from the experimental curve, considering negative and positive loading directions. The evolution of the stiffness-to-K_{ref} ratio curves is shown in Fig. 12. The initial stiffness of the pier that was strengthened on one side closely resembled that of the unstrengthened pier, while the pier strengthened on two sides exhibited a slightly higher initial stiffness (+22 %). The evolution shows an exponential decay, with a softer degradation in the strengthened samples.

3.3. Stiffness evaluation

The lateral stiffness of the walls from the experiment (K_{exp}) was compared with the analytical formula (Eq. (1)) proposed in [34]. The calculated values are reported in Table 6.

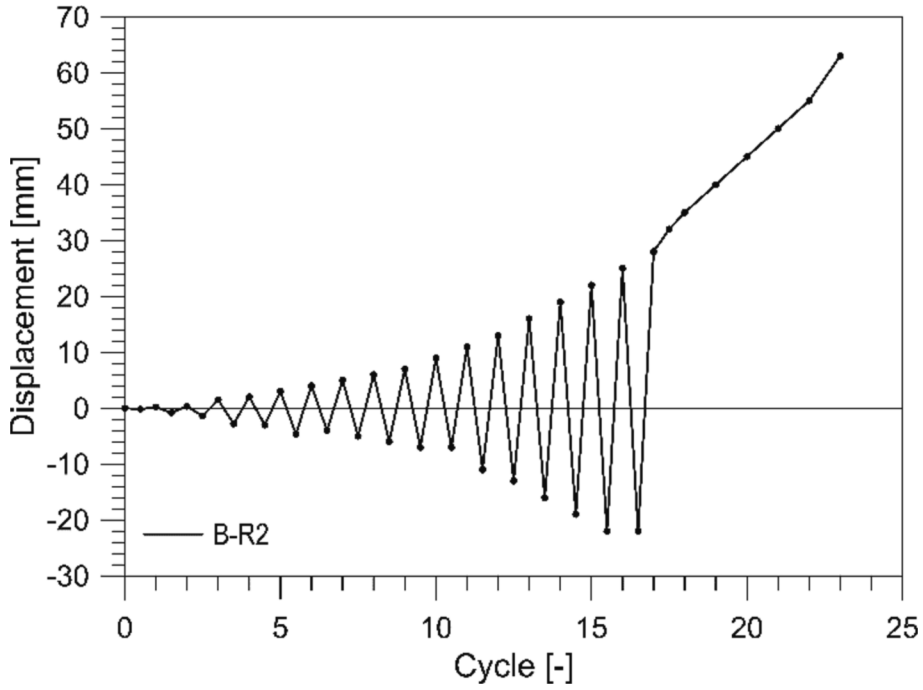

Fig. 9. Loading cycles for the pier B-R2.

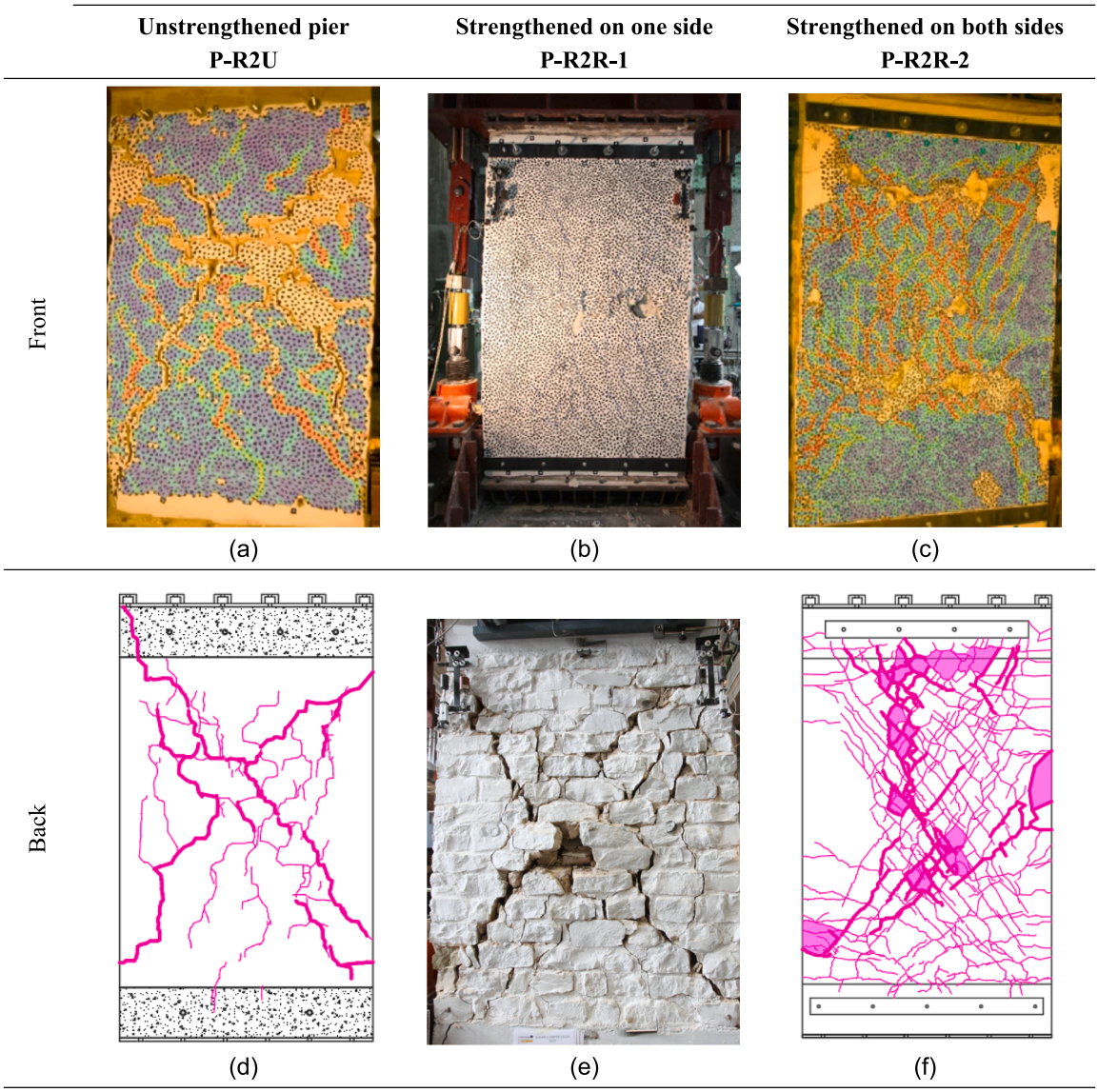

Fig. 10. Walls close to collapse – (a) front side of P-R2U by DIC (red denotes cracking), (b) front side of P-R2R-1, (c) front side of P-R2R-2 by DIC (red denotes cracking), (d) crack pattern at the back of P-R2U, (e) photo of the unstrengthened side of P-R2R-1 and (f) crack pattern at the back of P-R2R-2. (For interpretation of the references to colour in this figure legend, the reader is referred to the web version of this article.)

Table 4
Limit states of the piers.

	H_{cr} [kN]	Φ_{cr} [%]	H_{max} [kN]	Φ_{Hmax} [%]	H_{ult} [kN]	Φ_{ult} [%]
P-R2U	81	0.1	108	0.24	63	0.75
P-R2R-1	83	0.1	159	0.66	94	1.76
P-R2R-2	160	0.2	228	0.99	158	3.01

Note: H_{cr} = resistance at first cracking, Φ_{cr} = drift at first cracking, H_{max} = peak resistance, Φ_{Hmax} = drift at peak resistance, H_{ult} = resistance at near collapse, Φ_{ult} = drift at near collapse.

Table 5
Relative increase compared to the unstrengthened pier (P-R2U).

	H_{cr}	Φ_{cr}	H_{max}	Φ_{Hmax}	H_{ult}	Φ_{ult}
P-R2R-1	2 %	0 %	47 %	175 %	49 %	135 %
P-R2R-2	98 %	100 %	111 %	313 %	151 %	301 %

$$K = \frac{1}{\frac{1.2 \bullet h}{G_{eq} \bullet b \bullet t} + \frac{h^3}{E_{eq} \bullet J}} \quad (1)$$

where h, b and t are the height, width and thickness of the wall, respectively; J is the second moment of inertia; and E_{eq} and G_{eq} are the equivalent Young and shear moduli of the CRM-strengthened wall, respectively (evaluated as the weighted sum of the masonry and coating relative to the thickness of the unstrengthened wall).

The analytical predictions show a good alignment with the experimental values for the unstrengthened sample (P-R2U) and the sample strengthened on both sides (P-R2R-2). In the case of the pier strengthened on one side (P-R2R-1), the analytical model overestimates stiffness by 29 %, which is related to the initial cracking of the sample.

3.4. Energy dissipation

The capacity to dissipate energy during an earthquake is a crucial property of a structure. To evaluate the energy dissipation capacity, the cumulative input and hysteretic energies, E_{tot} and E_{hys}, respectively, were compared. The cumulative input energy E_{tot} was determined by

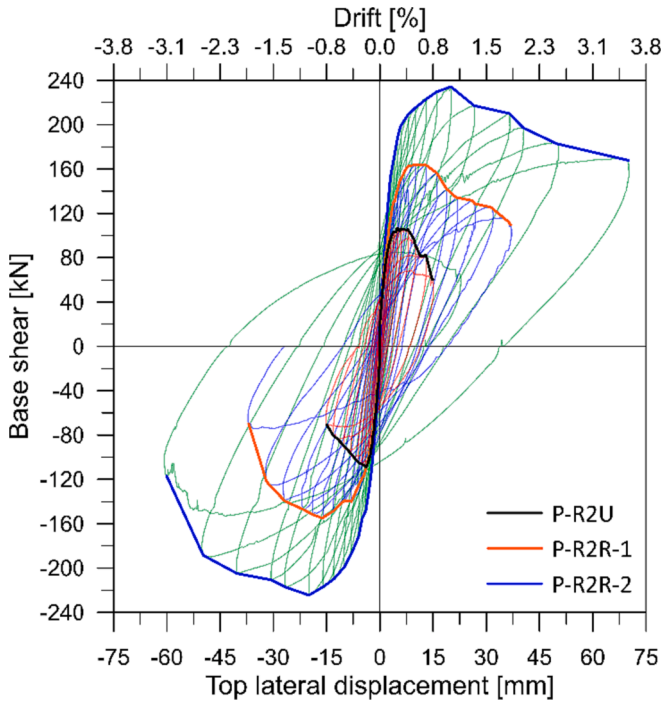

Fig. 11. Hysteretic response of piers in shear compression test and skeleton curves (unstrengthened, strengthened on one side and strengthened both sides).

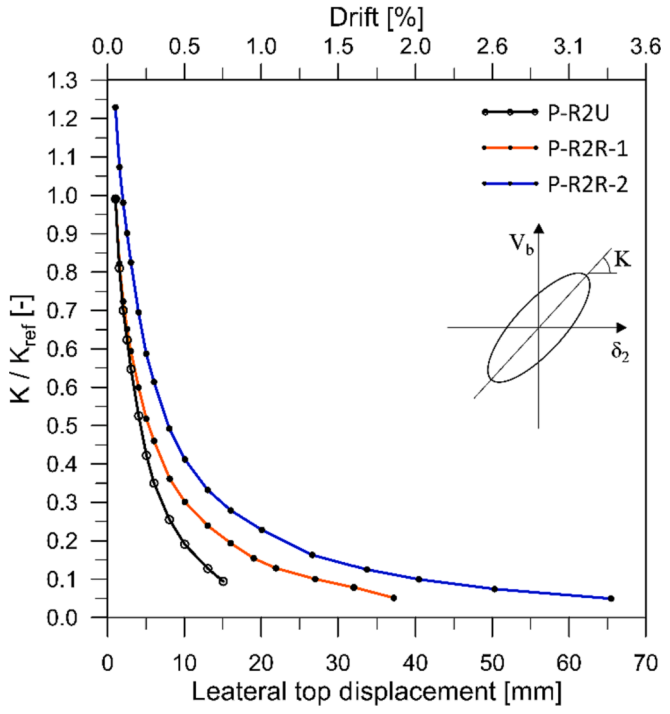

Fig. 12. Evolution of cycle lateral stiffness.

calculating the cumulative work required to deform the pier from the initial state to a specific displacement value during the test. This calculation requires the area under/over the positive/negative branches of the hysteretic loop for each loading cycle, while the cumulative dissipated hysteretic energy E_{hys} is determined by summing the areas enclosed by the hysteretic loops (Fig. 13).

Fig. 14 shows all three walls' dissipated and total energies. The energy dissipation capacity for total energy (E_{tot}) was 2.7 and 9.8 times

Table 6
Evaluation of the analytical lateral stiffness of the sample walls.

Sample	t_c [mm]	J [mm^4]	E_{eq} [MPa]	G_{eq} [MPa]	K [kN/mm]	K_{exp} [kN/mm]	K_{exp}/K
P-R2U	–	9.84E + 10	1074	430	61.1	59.7	0.98
P-R2R-1	30	1.07E + 11	1931	772	109.9	78.1	0. 71
P-R2R-2	2 × 30	1.15E + 11	2788	1115	158.7	134.9	0.85

Note:t_c is the thickness of the coating; E is Young's modulus of the masonry (E = 1074 MPa); G is the shear modulus of the masonry, considered as 0.4·E [32]; and E_c is Young's modulus of the coating (E_c = 10 091 MPa).

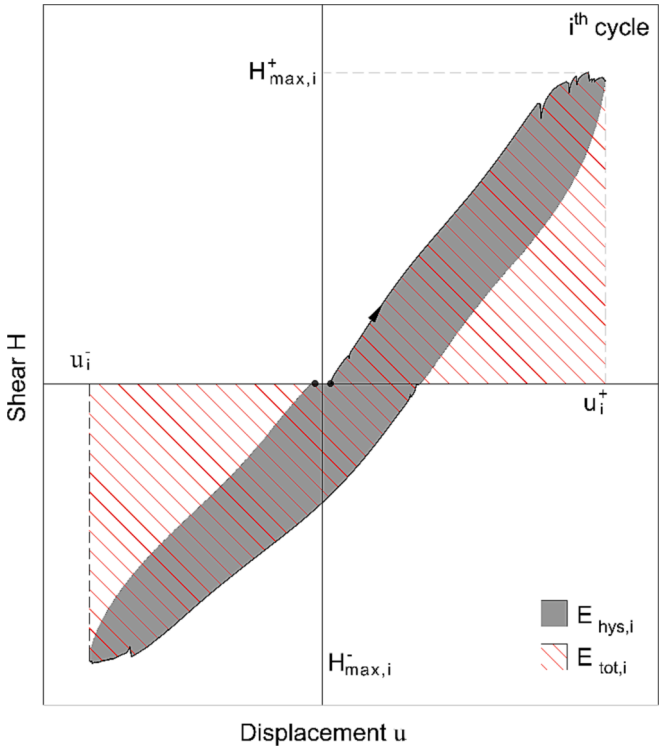

Fig. 13. Total and hysteretic energy.

higher for the walls reinforced on one side and two sides, respectively. The same numbers for hysteretic energy (E_{hys}) are 2.6 and 9.6. The increase in dissipation is entirely due to energy dissipated in the coating. The capacity of the coating to dissipate energy originates from the presence of reinforcement, which has tensile capacity and modifies damage pattern from localized to distributed (smeared) cracking. Smeared cracking is much more proficient in energy dissipation than localized cracking.

3.5. Equivalent viscous damping

The hysteretic response yields an approximate value of the equivalent hysteretic damping of the structure, which can be determined using the equation proposed by Chopra [33] and ATC FEMA 440 [34]:

$$\xi_{hys,i} = \frac{E_{hys,i}}{4\pi E_{s0,i}} \quad (2)$$

where $E_{hys,i}$ is the hysteresis energy dissipated within each cycle and $E_{s0,i}$ is the strain energy associated with the secant stiffness of the structure in the ith cycle, as illustrated in Fig. 13 and calculated using Eq. (3).

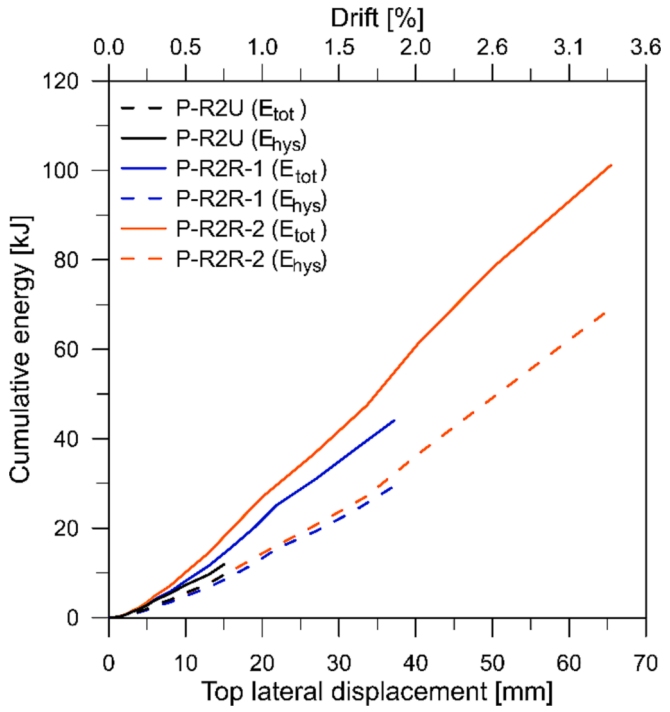

Fig. 14. Energy dissipation.

$$E_{s0,i} = \frac{1}{2} \bullet k_{s,i} \bullet \delta^2_{max,i} \quad (3)$$

where $k_{s,i}$ is the secant stiffness of the ith cycle (Fig. 12) and $\delta_{max,i}$ is the average of the positive and negative maximum displacements reached in the cycle.

Fig. 15 presents the evolution of the equivalent viscous damping calculated for the samples. The trends in ξ_{hys} among the samples are quite different. In the initial cycles, the unstrengthened sample exhibited a hysteretic damping of about 15 %, whereas the one- and two-side strengthened samples showed ξ_{hys} values of about 13 % and 10 %, respectively. The ξ_{hys} value was almost constant until 80–88 % of the peak load and then tended to increase until the end of the test, reaching about 33 % for the unstrengthened sample and roughly 25 % and 28 % for the one- and two-side strengthened samples, respectively.

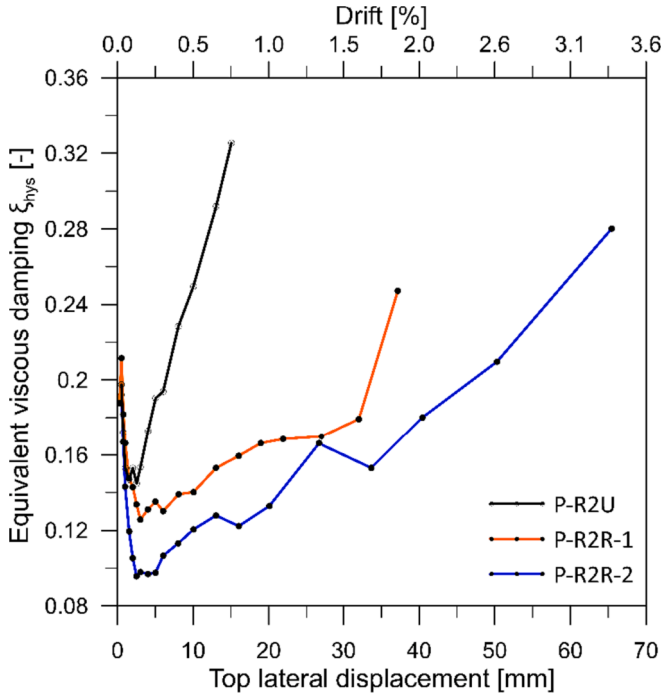

Fig. 15. Evolution of the equivalent hysteretic damping ratio ξ_{hys}.

3.6. Estimation of resistance to lateral load by CNR-DT 215/2018 (CNR, 2020) model

The Guide for the Design and Construction of Externally Bonded Fibre Reinforced Inorganic Matrix Systems for Strengthening Existing Structures, published by the National Research Council of Italy and commonly known as CNR-DT 215/2018 [35], proposes models for design. The strengthened masonry element's resistance must be checked for shear and bending resistance, and the guide provides analytical expressions for both models.

The shear model assumes that the shear resistance $V_{t,R}$ consists of the sum of the resistance of unreinforced masonry V_t according to the tensile strength model [36] and the contribution of the coating $V_{t,f}$ per Eq. (4). In this case, the strength of the unreinforced pier V_t is known from the test as 108 kN (Table 4). In calculating the contribution of coating, only the FRP material is considered, and mortar is neglected. The strength of the FRP is reduced because of exposure conditions, shear stress and the type of strengthening. Eq. (4) does not consider the reduction due to exposure conditions because the samples were built and stored in the laboratory and the test was performed soon after construction. Finally, the guidelines recommend a reduction due to coating on only one side of 30 %.

$$V_{t,f} = \frac{1}{\gamma_{Rd}} * \frac{F_s}{p} * l_f * \alpha_t \quad (4)$$

where γ_{Rd} is a factor equal to 2; F_s is the tensile resistance of one FRP strand; p is the grid pitch of 66 mm; l_f is the calculation size of the mesh, measured orthogonally to the shear force, and cannot be assumed greater than the dimension of the wall parallel to the shear force; and α_t is a factor accounting for the reduced extensional resistance of the fibres when subjected to shear.

The capacity of the pier in bending [35] is calculated based on the assumptions of planar sections, a perfect bond between the coating and the masonry, zero tensile strength of masonry, bilinear constitutive law for masonry in compression, and linear response of FRP until failure. The failure of FRP may be in different modes (e.g. fibre fracture, pull-out/sliding of fibres), which is considered in the equations by setting an appropriate value for ultimate strain in FRP. Because of the simplicity of the assumed constitutive relations, the guide provides analytical expressions for capacity in the appendix of the above-cited CNR recommendations. Three failure modes are given: compressive failure of masonry, tensile failure of FRP and bilinear compression in masonry, and tensile failure of FRP and elastic compression in masonry. The failure mode with the lowest capacity is the critical one. Alternatively, the equilibrium of the cross section can be calculated using the above assumptions.

The calculations according to the above assumptions are presented in Table 7, indicating very good alignment with the experiments. The engineering models predict the correct failure mechanisms and accurately estimate the capacity. The prediction for P-R2R-1, which had coating on one side and failed in shear, underestimates the capacity by 6.5 %. The prediction for P-R2R-2, which had coating on both sides and failed in bending, underestimates the capacity by 1.7 %.

3.7. Out-of-plane tests

3.7.1. Seismic response, collapse mechanisms and limit states

The stone masonry pier B-R2 was tested to OOP loads in a three-point bending loading scheme with cyclic load reversals. When pushed, the

Table 7
Capacity of the walls according to CNR/DT 215/2018.

Experiment	P-R2U	P-R2R-1	P-R2R-2
Resistance [kN]	108	159	228
Observed failure	diag. shear	shear	shear/bending
Model based on shear mechanism			
F_s [kN]		5.11	5.11
l_f [mm]		1500	1500
Reduction factor α_t (shear stress)		1.0	1.0
Reduction factor (coating on one side)		0.7	1
$V_{t,m}$ [kN]		108.0	
$V_{t,f}$ [kN]		40.6	116.1
$V_{t,R}$ [kN]		148.6	224.1
Model based on bending mechanism			
$V_{f,R}$ [kN]		193.6	228.4
Model prediction			
Capacity [kN]		148.6	224.1
Failure		shear	shear/bending*
Relative error [%]		−6.5	−1.7

Note: F_{strand}= ultimate capacity of a single mesh strand, $n_{strands}$ = number of strands in the direction perpendicular to the shear direction.
* Both mechanisms have very similar values, and the hybrid collapse was observed during the test.

coating was in tension, simulating the strengthened wall response; when pulled, the coating was in compression, which simulated the URM wall response.

The first crack occurred on the unreinforced side near the mid-height at $u = -2.8$ mm and a force of 6.5 kN. On the strengthened side, the first crack opened at $u = -3.0$ mm and 18.1 kN. As the displacement amplitudes increased, the crack pattern on the unstrengthened side remained the same as the single crack opened increasingly more (Fig. 17a). On the other hand, several new horizontal cracks opened on the strengthened side.

At $u = -22$ mm, the test was changed from cyclic to monotonic pushing. During this stage, the cracks in the coating multiplied and spread over almost the entire pier height (Fig. 16). The final collapse was due to the tensile failure of the GFRP mesh, as shown in Fig. 17b and c.

Fig. 18 presents the hysteretic response of the wall. The envelopes of the response in Fig. 18b clearly show the efficiency of strengthening, which increased resistance capacity by eight times. The coating and the wall performed as a composite element and resisted loads efficiently. The bond between the coating and the wall was not lost during the test. Because the GFRP mesh failed in tension, it was used to its full potential. Many cracks in the coating increased the capacity for energy dissipation

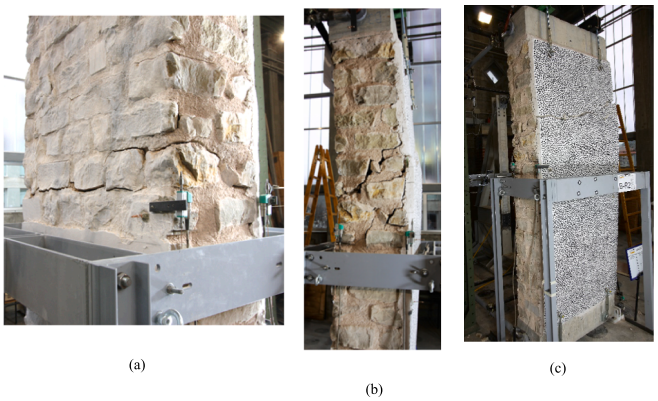

Fig. 17. (a) Crack on the unstrengthened side of the pier at − 22 mm and (b, c) final collapse of the pier.

compared to an unstrengthened pier, which had damage concentrated in just one major crack.

Fig. 19 compares the deformations at the mid-height of the pier on the strengthened and unstrengthened sides, surveyed with T12 and T13 instruments (Fig. 7b). First, the strength of the pier is clearly much larger when the coating is in tension. Second, the coating responds bilinearly in tension, and the stiffness changes at the formation of mortar cracks (which occur nearly simultaneously). In compression, on the other hand, the response differs very little, reaching high values of the masonry stress.

3.8. Estimation of the response

The moment capacity can readily be estimated once we realise that failure was due to the tensile rupture of the GFRP mesh. If a stress block distribution in compression is assumed (see Fig. 20), the calculation is straightforward because of the assumption of zero axial force. The moment capacity is provided by the moment couple C (compression) and T (tension), where T is the tensile strength of the GFRP mesh. For the evaluation of C, the location x of the neutral axis (n) is calculated first from the equilibrium of forces equation:

$$x = \frac{n_{strands} \bullet F_{strand}}{\beta \bullet b \bullet \alpha \bullet f_{m,c}} \tag{5}$$

where $f_{m,c}$ is the compressive strength of masonry, $\alpha = 0.85$ [32] and β is 0.7 [32].

Finally, the bending resistance capacity is calculated using Eq. (6).

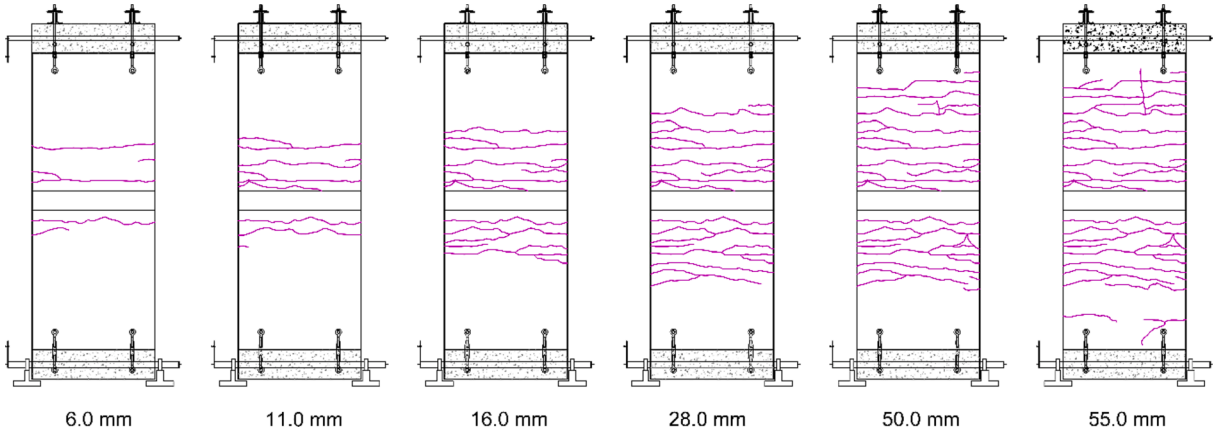

Fig. 16. Damage evolution on the strengthened side at different loading cycles.

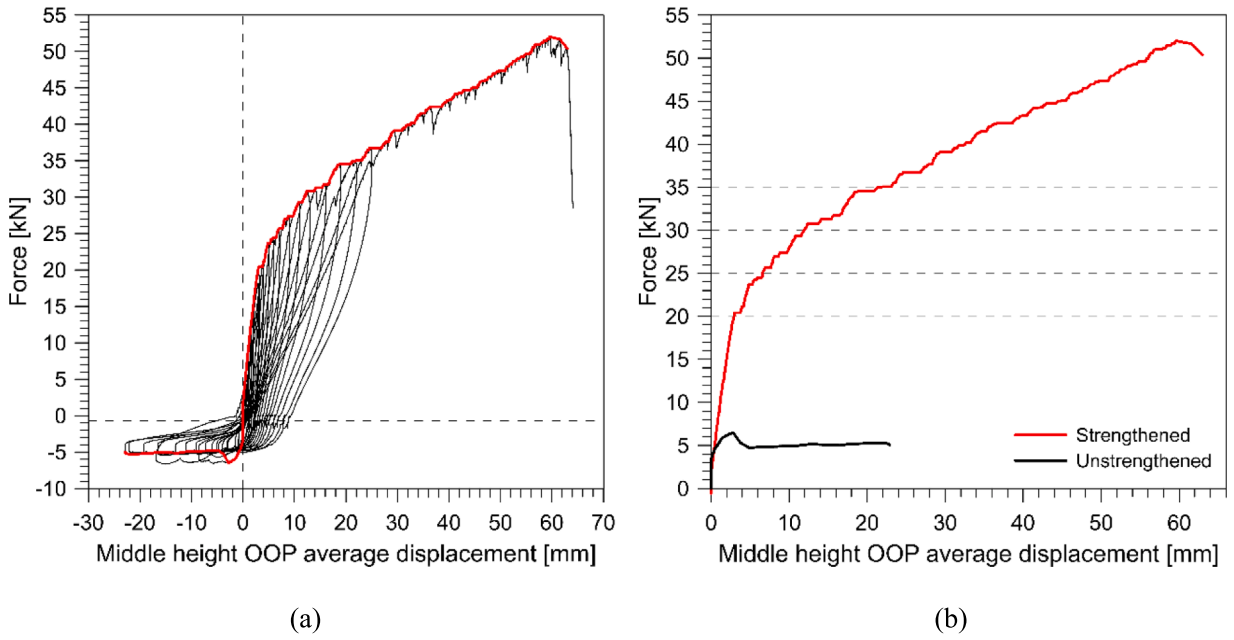

Fig. 18. (a) Response of the pier B-R2 to OOP loads and (b) envelopes of the response.

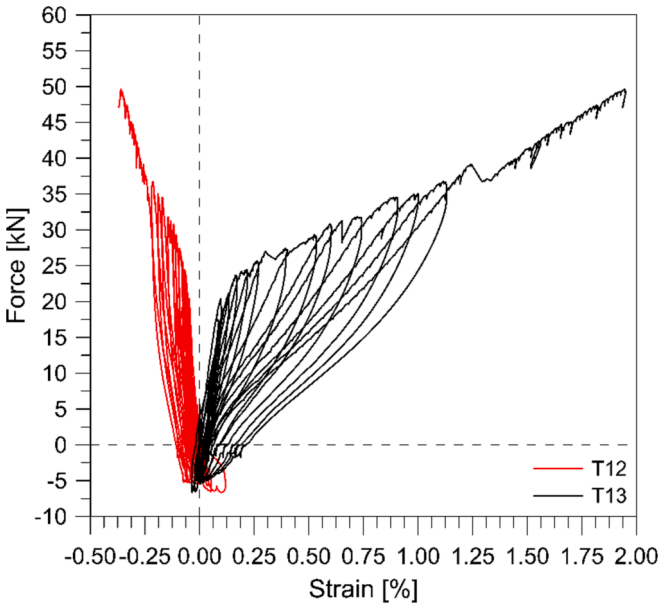

Fig. 19. Tensile deformation at mid-height (positive with crack opening).

$$M_{u(R)} = n_{strands} \bullet F_{strand} \hat{A} \cdot (t + \frac{t_c}{2} - \frac{\beta}{2} x) \quad (6)$$

The tested moment capacity is 35.5 kN·m, whereas the predicted capacity was 36.7 kN·m; thus, the model overestimates the capacity by 3.4 %, which can be explained by the slight variations in wall thickness along the height due to mortar joints and the shape of the stone blocks. The effective thickness may vary by 10–15 mm, and thus, the calculated capacity fits with the experimental result.

4. Conclusions

CRM strengthening of stone masonry walls with coating on only one side was analysed by experimental testing. The coating consisted of hydraulic lime mortar reinforced with GFRP mesh and two types of connectors. The full-scale experimental tests were performed on unstrengthened walls and walls strengthened on one and two sides. We conducted in-plane cyclic shear compression tests and OOP three-point bending cyclic tests. Existing design models were used to estimate the capacities observed in the tests, and a good alignment was observed.

As mentioned in the introduction, we did not know if CRM coatings on one side of the wall improve seismic response. The effect depends on the thickness and strength of CRM coating, the quality of the masonry, and the type of masonry connection. The strengthening technique is successful and efficient only if the coating and masonry are compatible and cooperate under seismic conditions as a composite element until collapse. Furthermore, to determine whether a method of strengthening is efficient requires experimental testing.

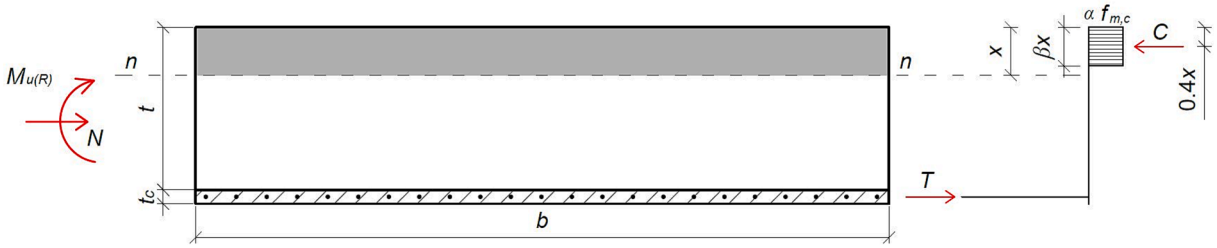

Fig. 20. Assumed stress state in the mid-height cross-section of the pier.

In the present case, the tests showed that the developed method of strengthening works with the considered historic two-wythe stone masonry. By strengthening the walls on one side, the following improvement were observed:

- In-plane resistance increased by 47 %, and displacement at maximum resistance rose by about 175 %.
- The capacity for energy dissipation improved about two and half times, and the ultimate displacement increased by 135 %.
- Debonding between coating and masonry was observed during the test, which eventually spread over the entire surface. However, because of the good connection, the coating and pier acted as a composite element until collapse. Therefore, proper connection is critical for seismic strengthening. At collapse, the GFRP mesh failed, indicating a desired collapse mechanism and that mesh was fully exploited.

OOP bending tests on piers strengthened on one side were performed to obtain information for design against local failures. The tests showed that the OOP resistance of strengthened walls is about eight times larger than that of unstrengthened walls and, thus, demonstrated that the developed method of strengthening helps prevent OOP failure.

If the coating is applied on both sides of the wall, it is effectively twice as strong. In-plane tests confirmed this since:

- The resistance to in-plane loads increased to 111 %, more than double that on only one side (47 %).
- The symmetrically positioned coating improved displacement capacity by 301 % and energy dissipation about tenfold.
- Debonding of the coating was observed, similarly as in the case of coating on one side. Again, the anchors provided a strong enough connection for the coating to be fully exploited and the response of the wall substantially improved.

The better performace indicates that strengthening on both sides is clearly the better system. Still, its drawback is that its application requires the temporary removal of the residents and higher costs.

The capacity of the proposed system was checked using a design model according to the CNR/DT guide. The estimate aligned well with the tests, with the relative errors for one or two sides strengthening of −6.5 % and −1.7 %, respectively. Furthermore, the design model correctly predicted the collapse mechanism. The model's accuracy confirms its use for the present system. Additionally, it validates the developed strengthening method, as the model's underlying assumptions about desired response are satisfied.

The developed method of strengthening on only one side was successful, but the improvement of seismic resistance was somewhat limited. Therefore, this one-side approach is suitable only in situations when such improvement is sufficient to achieve desired seismic resistance. Preliminary calculations show [1] that it could be enough for areas with small-to-medium seismic hazards but not enough for areas with high seismic hazards.

The key advantage of the proposed strengthening system is that it can be applied only on the outside and, therefore, does not affect residents or activities in the building. As a result, this solution may be appealing to more people who are otherwise not willing to strengthen their structures.

CRediT authorship contribution statement

Natalino Gattesco: Writing – review & editing, Supervision, Project administration, Methodology, Investigation, Funding acquisition. **Emanuele Rizzi:** Writing – original draft, Visualization, Investigation, Formal analysis, Data curation. **Ingrid Boem:** Writing – review & editing, Investigation. **Allen Dudine:** Writing – review & editing. **Matija Gams:** Writing – original draft, Project administration, Investigation, Formal analysis, Data curation.

Declaration of Competing Interest

The authors declare that they have no known competing financial interests or personal relationships that could have appeared to influence the work reported in this paper.

Data availability

Data will be made available on request.

Acknowledgements

The experimental tests presented were carried out within the project CONSTRAIN, partially funded by the Interreg Italy-Slovenia Cooperation Program 2014-2020 and led by the University of Trieste, Italy, alongside the University of Ljubljana (Slovenija) and the companies Fibre Net S.p.A., Igmat d.d., Veneziana Restauri Costruzioni S.r.l. and Kolektor CPG d.o.o. The support of the Slovenian Research Agency (project P2-0185) is also gratefully acknowledged.

References

[1] N. Gattesco *et al.*, «The Experimental Campaign and Numerical Simulations of the CONSTRAIN Project. Technical report. Standard project co-fincanced by the European Regional Development Fund.» 2022.
[2] T. Petrovski, «Damaging Effects of July 26, 1963 Skopje Earthquake», *MESF Cyber J. Geosci.* vol. 2, gen. 2004.
[3] M. Santulin, et al., The legacy of the 1976 Friuli earthquake, Boll. Geofis. Teor. Ed Appl. 59 (2018) 543–558, https://doi.org/10.4430/bgta0228.
[4] R. Marques, «Masonry Box Behavior», in *Encyclopedia of Earthquake Engineering*, M. Beer, I. A. Kougioumtzoglou, E. Patelli, e I. S.-K. Au, A c. di, Berlin, Heidelberg: Springer, 2021, pp. 1–18. doi: 10.1007/978-3-642-36197-5_155-1.
[5] M. Tomaževič, Earthquake-resistant design of masonry buildings, Imperial College Press, 1999.
[6] D. Benedetti, P. Carydis, e P. Pezzoli, «Shaking table tests on 24 simple masonry buildings», *Earthq. Eng. Struct. Dyn.*, vol. 27, fasc. 1, pp. 67–90, 1998, doi: 10.1002/(SICI)1096-9845(199801)27:1<67::AID-EQE719>3.0.CO;2-K.
[7] CEN, «EN 1998-1:2004/A1:2013 - Eurocode 8: Design of structures for earthquake resistance - Part 1: General rules, seismic actions and rules for buildings», iTeh Standards. Consultato: 13 gennaio 2023. [Online]. Disponibile su: https://standards.iteh.ai/catalog/standards/cen/74f615b9-4800-4e6e-b9a4-2d8c8b83142d/en-1998-1-2004-a1-2013.
[8] G. Croci, D. D'Ayala, P. D'Asdia, e F. Palombini. «Analysis on shear walls reinforced with fibres». In: *IABSE Symp. on Safety and Quality Assurance of Civil Engineering Structures*. 1987.
[9] T. Triantafillou e M. N. Fardis. «Advanced composites as strengthening materials of historic structures». In: *IABSE Symp. on Structural Preservation of the Architectural Heritage*. 1993.
[10] C.G. Papanicolaou, T.C. Triantafillou, K. Karlos, e.M. Papathanasiou, Textile-reinforced mortar (TRM) versus FRP as strengthening material of URM walls: in-plane cyclic loading, Mater. Struct. 40 (fasc. 10) (2007) 1081–1097, https://doi.org/10.1617/s11527-006-9207-8.
[11] T. Triantafillou. «Strengthening of Masonry Structures Using Epoxy-Bonded FRP Laminates». *J. Compos. Constr. - J COMPOS CONSTR.* vol. 2. mag. 1998. doi: 10.1061/(ASCE)1090-0268(1998)2:2(96).
[12] M. Gams, M. Tomaževič, e.T. Berset, Seismic strengthening of brick masonry by composite coatings: an experimental study, Bull. Earthq. Eng. 15 (2017) ott, https://doi.org/10.1007/s10518-017-0136-4.
[13] C.G. Papanicolaou, T.C. Triantafillou, K. Karlos, e.M. Papathanasiou, Textile-reinforced mortar (TRM) versus FRP as strengthening material of URM walls: in-plane cyclic loading, Mater. Struct. 40 (fasc. 10) (2007) 1081–1097, https://doi.org/10.1617/s11527-006-9207-8.
[14] C.G. Papanicolaou, T.C. Triantafillou, M. Papathanasiou, e.K. Karlos, Textile reinforced mortar (TRM) versus FRP as strengthening material of URM walls: out-of-plane cyclic loading, Mater. Struct. 41 (fasc. 1) (2007) 143–157, https://doi.org/10.1617/s11527-007-9226-0.
[15] S. De Santis, F.G. Carozzi, G. de Felice, e.C. Poggi, Test methods for Textile Reinforced Mortar systems, Compos. Part B Eng. 127 (2017) 121–132, https://doi.org/10.1016/j.compositesb.2017.03.016.
[16] L.A. S. Kouris, e.T.C. Triantafillou, State-of-the-art on strengthening of masonry structures with textile reinforced mortar (TRM), Constr. Build. Mater. 188 (2018) 1221–1233, https://doi.org/10.1016/j.conbuildmat.2018.08.039.
[17] I. Boem, e.N. Gattesco, Characterization of Textile-Reinforced Mortar: State of the Art and Detail-Level Modeling with a Free Open-Source Finite-Element Code, J. Compos. Constr. 26 (fasc. 5) (2022) 04022060, https://doi.org/10.1061/(ASCE)CC.1943-5614.0001240.

[18] I. Boem, Masonry Elements Strengthened with TRM: A Review of Experimental, Design and Numerical Methods, Buildings 12(9) (2022) 1307, https://doi.org/10.3390/buildings12091307.
[19] A. D'Ambrisi, M. Mezzi, e.A. Caporale, Experimental investigation on polymeric net-RCM reinforced masonry panels, Compos. Struct. 105 (2013) 207–215, https://doi.org/10.1016/j.compstruct.2013.05.017.
[20] L. Garcia-Ramonda, L. Pelà, P. Roca, e.G. Camata, Cyclic shear-compression testing of brick masonry walls repaired and retrofitted with basalt textile reinforced mortar, Compos. Struct. 283 (2022), 115068, https://doi.org/10.1016/j.compstruct.2021.115068.
[21] N. Ismail, e.J.M. Ingham, In-plane and out-of-plane testing of unreinforced masonry walls strengthened using polymer textile reinforced mortar, Eng. Struct. 118 (2016) 167–177, https://doi.org/10.1016/j.engstruct.2016.03.041.
[22] A. Bellini, A. Incerti, M. Bovo, e C. Mazzotti, Effectiveness of FRCM Reinforcement Applied to Masonry Walls Subject to Axial Force and Out-Of-Plane Loads Evaluated by Experimental and Numerical Studies, Int. J. Archit. Herit. 12 (fasc. 3) (2018) 376–394, https://doi.org/10.1080/15583058.2017.1323246.
[23] J. Proença, A.S. Gago, J. Cardoso, V. Cóias, e.R. Paula, Development of an innovative seismic strengthening technique for traditional load-bearing masonry walls, Bull. Earthq. Eng. 10 (fasc. 1) (2012) 113–133, https://doi.org/10.1007/s10518-010-9210-x.
[24] M. Del Zoppo, M. Di Ludovico, e A. Prota, Analysis of FRCM and CRM parameters for the in-plane shear strengthening of different URM types, Compos. Part B Eng. 171 (2019) 20–33, https://doi.org/10.1016/j.compositesb.2019.04.020.
[25] G. Roselli, et al., Mortar analysis of historic buildings damaged by recent earthquakes in Italy, Eur. Phys. J. plus 134 (2019) 540, https://doi.org/10.1140/epjp/i2019-13024-2.
[26] CEN. «EN 1015-11:2019 - Methods of test for mortar for masonry - Part 11: Determination of flexural and compressive strength of hardened mortar», iTeh Standards. Consultato: 13 gennaio 2023. [Online]. Disponibile su: https://standards.iteh.ai/catalog/standards/cen/14596d4c-119b-4a78-94e1-3fe481a29bde/en-1015-11-2019.
[27] CEN. «EN 1052-1:1998 - Methods of test for masonry - Part 1: Determination of compressive strength», iTeh Standards. Consultato: 20 marzo 2023. [Online]. Disponibile su: https://standards.iteh.ai/catalog/standards/cen/1b839a8c-0f0a-4398-b6e2-293984753dd0/en-1052-1-1998.
[28] CEN. «EN 12390-13: Testing hardened concrete - Part 13: Determination of secant modulus of elasticity in compression». CEN/TC 104, CEN/TC 104/SC1. 2021.
[29] ISO. «ISO 10406-1: Fibre-reinforced polymer (FRP) reinforcement of concrete — Test methods — Part 1: FRP bars and grids». ISO/TC 71/SC 6. 2008.
[30] M. Tomaževič, M. Gams, e T. Berset, Strengthening of stone masonry walls with composite reinforced coatings, Bull. Earthq. Eng. 13(fasc. 7) (2015) 2003–2027, https://doi.org/10.1007/s10518-014-9697-7.
[31] M. Tomaževič, M. Lutman, e L. Petković, «Seismic Behavior of Masonry Walls: Experimental Simulation», *J. Struct. Eng.*, vol. 122, fasc. 9, pp. 1040–1047, set. 1996, doi: 10.1061/(ASCE)0733-9445(1996)122:9(1040).
[32] NTC, «Decreto 17 gennaio 2018: Aggiornamento delle "Norme tecniche per le costruzioni".» Italian Ministry of Infrastructure and Transport, Rome, Italy. 20 febbraio 2018.
[33] A.K. Chopra, Dynamics of structures: theory and applications to earthquake engineering, 4th ed., Prentice Hall, Upper Saddle River, N.J, 2012.
[34] ATC FEMA 440. *ATC FEMA 440: Improvement of Nonlinear Static Seismic Analysis Procedures*. 2005.
[35] CNR, «CNR-DT 215/2018 Guide for the Design and Construction of Externally Bonded Fibre Reinforced Inorganic Matrix Systems for Strengthening Existing Structures». CNR, 2020. [Online]. Disponibile su: https://www.cnr.it/en/node/12827.
[36] Turnšek V. e Čačovič F, «Some experimental results on the strength of brick masonry walls», *HWH West KH Speed Br. Ceram. Reasearch Assoc. - Lond. Ed. Proc. 2nd Int. Brick-Mason. Conf. Stoke–Trent UK Br. Ceram. Res. Assoc*. 149–156. 1971.